21st International Conference on Composite Materials
Xi'an, 20-25th August 2017

CAPTURING SUBTLE FEATURES OF DELAMINATION SHAPES IN CROSS-PLY LAMINATES DUE TO LOW SPEED IMPACT

Elena Sitnikova [1*], Shuguang Li [1], Dafei Li [1] and Xiaosu Yi[2]

[1] Faculty of Engineering, The University of Nottingham, University Park, Nottingham NG7 2RD, UK
[2] Beijing Institute of Aeronautical Materials, Wenquan, Haidian District, Beijing, 100095, China
*Presenting author's email: elena.sitnikova@nottingham.ac.uk

Keywords: Laminate; Delamination, Matrix cracking; Damage mechanics; Friction

ABSTRACT

The present paper is to enhance the understanding of general delamination problem by addressing a few basic phenomena which have been well-observed repeatedly, but hardly comprehended, let alone being captured via the theoretical modelling. Specifically, in cross-ply laminates, the shape of delamination areas, which form due to low velocity impact, has two subtle features, which have been captured consistently in numerous experiments, but have not been reproduced consistently through numerical modelling. Those are the pointed delamination tips and the intact zone between the lobes of delamination. Out of the present investigation, these features have been subjected to close examination. In each case, a key and unique reason has been identified.

1 INTRODUCTION

Delamination in laminated composites caused by low speed lateral impact has been subjected to countless investigations from various perspectives [1], to such an extent that standards [2] have been drawn, as the problem has been considered as one of the key aspects in material selection, in particular, for aerospace applications.

Cross-ply laminates are one of the simplest types of laminates, which is not of much practical significances in terms of their engineering applications. However, their simplicity makes them an ideal case of verifications and validations of theoretical models. They have indeed been employed frequently as one of the benchmarking cases [3]. Experimental results based on different materials are found highly reproducible and consistent [4-6]. Most of the prominent features of delamination are captured well through carefully conducted numerical simulations. Reasonable agreement between the experimentally observed and numerically predicted delamination, both qualitative and quantitative, has been reported by many [5, 7 - 9]. More research outcomes are still being reported [10-14], which suggests the need of better understanding before composites can be applied with higher level of fidelity, the lack of which in relation to the extensive use of composites in Boeing 787 was clearly identified in the report from a US government public enquiry [15].

Most of the prominent features of delamination in cross-ply laminates are easily reproducible experimentally. Some of them have been employed as the measure of the extent of damage, e.g. the dimensions of the delamination, its area, etc. Though a reasonable agreement between the experiment and modelling is usually reported, there is still lack of understanding as to what effect the various factors included in modelling have on delamination predictions. Another closely associated and even more important issue is the inability to comprehensively explain two subtle features of delamination as will be defined below, which are observed consistently in impact tests of cross-ply laminates, but are not captured in many accounts exploring the subject.

2 TWO SUBTLETIES CONCERNED

Consider the relatively best known case of cross-ply laminates of a layup $[0°_m/90°_n/0°_m]$ subjected to impact. It can be easily predicted, as well as experimentally observed, that the delamination on the proximal, 0°/90°, interface closer to the impactor does not propagate much, and the observed delamination is dictated by the one on the distal, 90°/0°, interface farther from the impactor, from which the delamination area and dimensions are measured. The peanut shape of the delamination has been

well-observed experimentally and predicted theoretically. However, there are two subtle features that have never been understood appropriately.

(1) The tips of delamination at both ends tend to be pointed, as consistently observed in experiments. The predictions, however, turn out to be either too blunt to miss the pointed feature completely, or too needle-shaped to be realistic.

(2) The other observation is an intact zone between the two lobes of the delamination. The so-called intact zone is usually not entirely damage free. In fact, complicated damage patterns can usually be observed there as a result of localised indentation due to the impact. However, as far as the interface is concerned, the delamination does not propagate into this zone. Again, it is a consistently observed feature of the delamination.

A schematic sketch of the delaminated zone as is typically captured experimentally [4,6] is shown in Figure 1, with the two features as mentioned above being marked in the figure.

There has probably no lack of interest in capturing these features as they are so characteristic and reproducible in experiments. However, the fact is that there has not yet been a conclusive statement about their being and the reasons behind such distinctive mechanisms of delamination. Although one may claim that in representing the effects of the delamination, such subtle features are not as significant as the delamination area and dimensions, the inability to capture them does cast doubts on the fidelity of the means of the predictions, even if one has managed to get the area and the overall dimensions reasonably accurately.

The objective of this paper is to address these subtleties. Through the specific considerations introduced to the modelling as presented in this paper, these subtle features will not only be reproduced vividly, but also the reasons responsible for these features will be revealed.

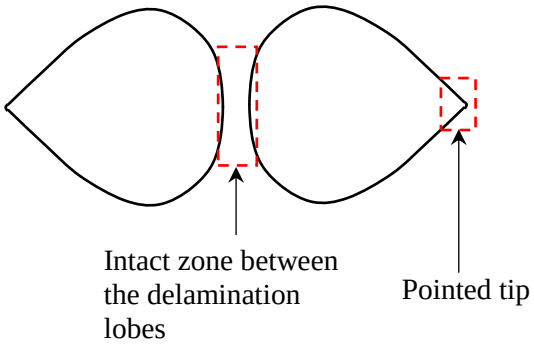

Figure 1. Schematic drawing of typical delamination pattern in the distal interface of $[0°_m/90°_n/0°_m]$ laminate captured experimentally

3 MODELLING IMPACT ON CROSS-PLY LAMINATE

In the present investigation, delamination due to low velocity impact on cross-ply laminate with $[0_3/90_3]_s$ lay-up is studied via a finite element modelling conducted with Abaqus/Explicit [16]. The finite element model was generated in order to compare directly with the laminated panel impact experiments [6,9].

3.1 Finite element model

In experiments [6,9], the $[0_3/90_3]_s$ laminate was 2mm thick, with 65mm×87.5mm in-plane dimensions. The laminate panel was simply supported. The simple support conditions in experiments were obtained by resting the specimen on a rigid steel plate with a rectangular cut-out of an area 45mm×67.5mm with all four corners of the specimen clamped at positions close to the edge of the cut-out. The clamps were to ensure zero deflection at the corners. The specimen was impacted in the centre by a hemispherical impactor 12.5 mm in diameter, which was considered as a rigid body. Impacts of

different energies were simulated by assigning appropriate velocity values to the impactor at the instant of contact. The mass of the impactor in the tests was 2.3 kg.

To reduce the computational costs, only a quarter of the specimen was modelled, with appropriate symmetry conditions being imposed, as specified in Figure 2(a). The composite laminate was comprised of three layers, each consisting of plies having a common orientation as shown in Figure 2(b). The interfaces between the composite layers were modelled by cohesive elements COH3D8. The unidirectional composite layers were meshed with continuum shell elements, SC8R. The surface-to-surface contact interactions were defined between the plate and the indenter, and also on the faces of the contacting composite layers, to prevent upper lamina penetrating lower lamina following the failure of the cohesive layer. Since the analysis for conducted with a quarter of the panel, the mass of the impactor was also reduced to a quarter in the model

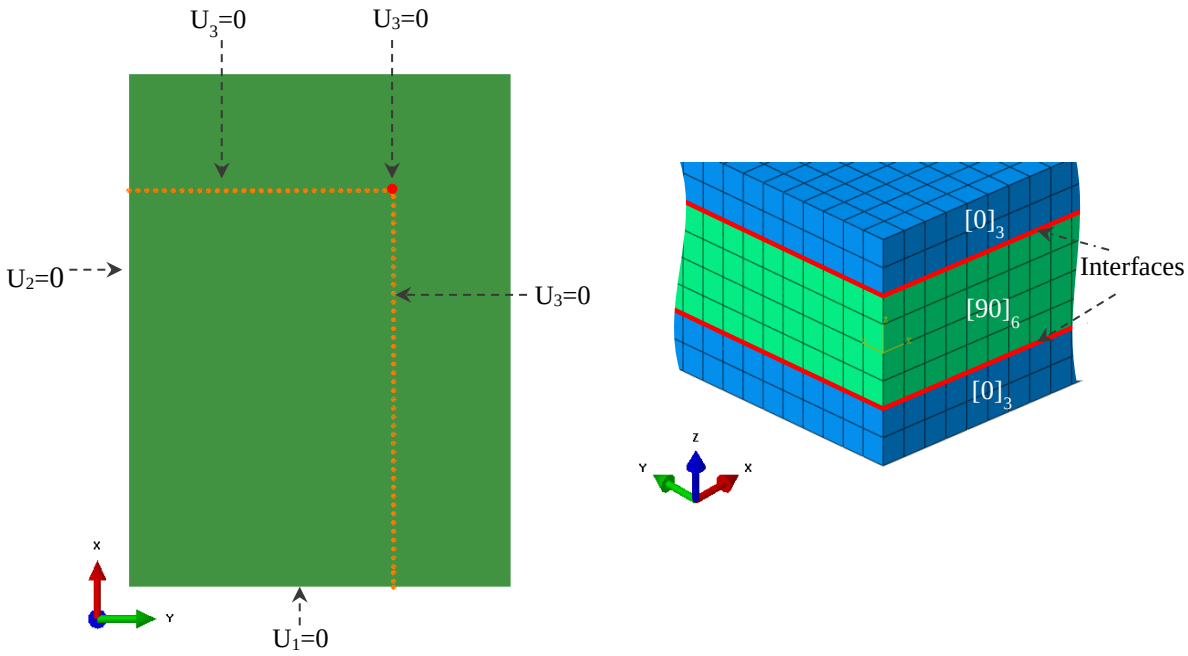

(a) (b)

Figure 2. Finite element model of the laminate: (a) bottom view of the quarter of the panel with the boundary conditions specified (b) close-up image of the centre of the panel

Given the mesh sensitivity of delamination problems in general, a study has been conducted to determine the mesh convergence which was reached when both the composite and the cohesive layers were meshed with elements of 0.25 mm×0.25mm in-plane dimensions with the through-the-thickness arrangement as shown in Figure 2(b).

3.2 The constitutive behaviour of cohesive interfaces

The elastic behaviour of the interface is defined in terms of tractions (t_n, t_s and t_t) and separations (δ_n, δ_s and δ_t) relationship, which are expressed in local coordinate system of the cohesive element as [16]

$$\begin{Bmatrix} t_n \\ t_s \\ t_t \end{Bmatrix} = \frac{1}{T}\begin{bmatrix} K_{nn} & 0 & 0 \\ 0 & K_{ss} & 0 \\ 0 & 0 & K_{tt} \end{bmatrix}\begin{Bmatrix} \delta_n \\ \delta_s \\ \delta_t \end{Bmatrix}, \tag{8}$$

where T is the thickness of the cohesive layer and K_{nn}, K_{ss} and K_{tt} represent the stiffness characteristics of the interface in normal and two perpendicular tangential directions to the interface. The interface stiffnesses are introduced as the penalty functions, which are employed to impose the relevant constraints numerically.

Damage initiation is governed by a quadratic interfacial traction criterion, which is defined as follows:

$$\left(\frac{\langle t_n \rangle}{t_n^c}\right)^2 + \left(\frac{t_s}{t_s^c}\right)^2 + \left(\frac{t_t}{t_t^c}\right)^2 = 1, \tag{9}$$

where t_n^c, t_s^c and t_t^c are the peak nominal stresses in normal and tangential directions, and $\langle\ \rangle$ are the Macaulay brackets.

To define the damage evolution, a power law criterion for mixed mode delamination is employed, which is given as

$$\left(\frac{G_I}{G_{Ic}}\right)^{\alpha} + \left(\frac{G_{II}}{G_{IIc}}\right)^{\beta} + \left(\frac{G_{III}}{G_{IIIc}}\right)^{\gamma} = 1, \tag{10}$$

where G_I, G_{II} and G_{III} represent the fracture energies for each of three individual modes and G_{Ic}, G_{IIc} and G_{IIIc} are their critical values. The values of exponents in Eq. (10) were chosen to be $\alpha = \beta = \gamma = 1$.

The damage evolution law governs the behaviour of the interface in terms of the degradation of the interface stiffness. A non-dimensional scalar damage variable, *D*, is defined via linear softening scheme [16]. The material properties required for the use of cohesive elements are presented in Table 1.

Table 1.The material properties of the cohesive layers [9]

K_{nn} =120GPa/mm;	$K_{ss} = K_{tt}$ =48GPa/mm
t_n^c =30MPa;	$t_s^c = t_t^c$ =80MPa
G_{Ic} =520J/m^2,	$G_{IIc} = G_{IIIc}$ =970J/m^2

After running the trial impact simulations, it became apparent that along with the delamination at the distal interface, delamination was also predicted at the proximal 0°/90° interface. This is due a shortcoming of the cohesive material model [16], which simply disregards the contribution of the compressive normal stress, allowing the shear-driven delamination to propagate unaffected by the presence of the direct compression. In present work, to save computational costs, the delamination at the upper interface was artificially suppressed.

Unless otherwise specified, the predicted delamination patterns are presented as contours of damage variable, *D*, which were plotted using Abaqus post-processing tool. The threshold value *D*=0.9 was set, so that the contour would delimit the area where nearly complete failure of the cohesive elements occurred.

3.3 Constitutive model for the composite lamina taking account of intra-laminar damage

To account for the effect of the matrix cracking on the response of the composite layers, damage model [17, 18] was employed to define the mechanical response of the composite.

The constitutive relationship for the laminae is given as follows.

$$\{\sigma\} = [Q]\{\varepsilon\}, \tag{1}$$

where Q is the laminar stiffness matrix which is in general a function of damage variable, ω.

An incremental form of Eq. (1) is obtained as

$$\{d\sigma\} = [Q^t]\{d\varepsilon\}, \tag{2}$$

where

$$\begin{gathered}[Q^t] = [Q^\omega] + \frac{[Q^\omega]\{\varepsilon\}\dfrac{\partial F}{\partial\{\sigma\}}[Q^\varepsilon]}{h\eta\omega^{\eta-1} - \dfrac{\partial F}{\partial\{\sigma\}}[Q^\omega]\{\varepsilon\}}, \\ Q_{ij}^\varepsilon = Q_{ij} + Q'_{ij}\omega, \\ Q_{ij}^\omega = Q'_{ij} \quad (i,j=1,2), \\ Q_{66}^\varepsilon = (1-k\omega)G \quad \text{and} \quad Q_{66}^\omega = -kG. \end{gathered} \tag{3}$$

In Eq. (3), G is the elastic in-plane shear modulus of virgin material and k is a damage-related laminate constant [17]. The expressions for Q_{ij} and Q'_{ij} in terms of conventional elastic constants can be found in [18] as a simplified version of continuum damage representation proposed by Talreja [19].

For simplicity, the damage initiation was defined via the maximum stress failure criterion, which is written as follows.

$$F(\sigma) = \frac{\sigma_2}{\sigma_{2c}} \tag{4}$$

where σ_{2c} is the transverse strength within the lamina.

The evolution of damage is given in an incremental form as [18]

$$d\omega = \left(h\eta\omega^{\eta-1} - \frac{\partial F}{\partial\{\sigma\}}[Q^\omega]\{\varepsilon\}\right)^{-1}\frac{\partial F}{\partial\{\sigma\}}[Q^\varepsilon]\{d\varepsilon\}. \tag{5}$$

It was derived based on the concept of the damage surface, which was defined in the following form [18]

$$f(\sigma,\omega) = (1+h\omega^\eta)^{-1}F(\sigma) = 1, \tag{6}$$

where h and η are properties of the material of lamina associated with the size effects of the material. Unloading is characterised by $d\omega$ becoming negative, in which case Eqs. (3) and (5) are replaced by

$$[Q^t]=[Q^\varepsilon] \quad \text{and} \quad d\omega = 0. \tag{7}$$

The elastic constants and other relevant material properties of the composite are listed in Table 1. To define the response of the material with the damage, two additional quantities, h and η, need to be specified.

Table 2. Material properties of unidirectional Seal HS160/REM/graphite/epoxy [9]

E_{11}=93.7GPa; E_{22}= E_{33}=7.45GPa
G_{12}= G_{23}= G_{13}=3.97GPa
ν_{12}= ν_{23}= ν_{13}=0.261
σ_{2c} =30MPa
ρ=1600 kg/m^3

The damage model was implemented as a user-defined VUMAT subroutine. To verify the damage model implementation, typical material responses under transverse loading were calculated based on a single element model. In Figure 3, several stress-strain curves are presented, corresponding to different combinations of parameters h and η. As can be seen, in all the cases, the curve starts to deviate from a linear elastic response once the damage initiation threshold of 30 MPa was reached. At values of h and η greater than zero, material exhibits strain hardening-like response following the damage initiation. On the other hand, at values of h<0 rapid stiffness reduction is observed following the initiation of damage. This is consistent with Eq. (6), which suggests that the damage threshold for further damage at every

increment should reduce if h is negative, and increase otherwise. Since the values for parameters h and η were not available, to facilitate the modelling, they were assumed to be equal to zero in all the simulations, unless otherwise specified. This corresponds to ideally plastic-like material response (blue curve), also shown in Figure 3, that gives the simplest stress-strain characterization, incorporating a degree of load carrying capacity of the cracked laminae whilst keeping the relationship as simple as possible. The unloading and re-loading scenarios are included.

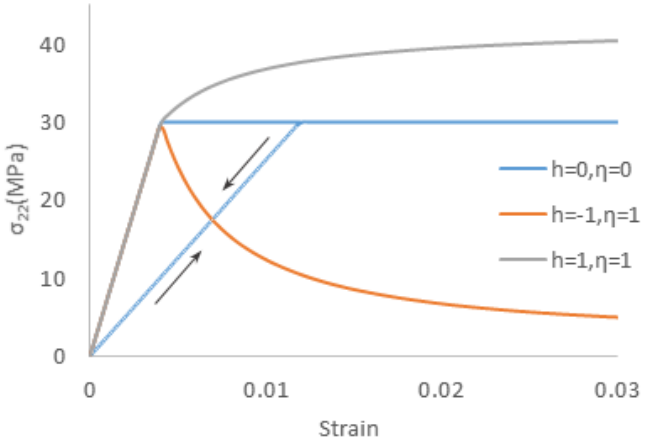

Figure 3: Stress-strain curves obtained with a single element FE model at different values of h and η

The value of constant k in Eq. (3), defining the reduction of shear stiffness due to damage [17], was assigned a value of $k = 0.75$.

4 CAPTURING THE FEATURE OF POINTED DELAMINATION TIP

Using the finite element model as described in the previous section, low velocity impact simulations were conducted. To assess and compare the effects different methods of composite damage modelling have on the delamination predictions in the 90°/0° interface, low velocity impact simulations were conducted with three different models in the present study:

1) The response of the composite laminae was assumed to be entirely elastic and the intra-laminar damage was not accounted for in any form;
2) Composite cracking was modelled by placing a layer of interface elements on the symmetry plane of the distal 0° lamina to allow the discrete crack, which would have the effects of all cracks, macroscopic and microscopic, lumped to it; and
3) CDM-based formulation, as described in Section 2.2, is employed to model the effects of intra-laminar damage.

The predictions obtained with three methods listed above are shown in Figure 4(a)-(c), respectively. The delamination patterns obtained from the three models can be compared from different perspectives. A general 'peanut'-shaped pattern can be observed in all of them. However, for purely elastic composite response, delamination exhibits conspicuous rounded profile at both ends, as shown Figure 4(a), while pointed tips at the end of each delamination lobe are apparent in Figure 4(b), where intra-laminar damage is represented by a discrete crack. In Figure 4(c), where the intra-laminar damage is modelled as continuum, and hence is considered dispersed, along with other minor changes, the tips changed towards pointed appearance, although not as pronounced as in Figure 4(b). To allow for the direct comparison of the delamination shapes obtained with above different methods of modelling damage in the composite, delamination patterns calculated at impact energy 7J are superimposed in Figure 5. The smallest delamination area was predicted for the model which does not account for intra-lamina damage. For a model with an embedded discrete crack (yellow curve), the length of delamination is substantially larger than in the previous case, while the width remains similar. With CDM to account for intra-laminar damage, two delamination patterns are presented, which were obtained with different values of

parameters h and η, defining the shape of the damage surface. In both cases, the tendency of pointed delamination tips as a distinct feature of the delamination has been captured. Along with this feature, the delamination area becomes larger. This increase tends to coincide with the degradation of composite stiffness as introduced by the CDM model.

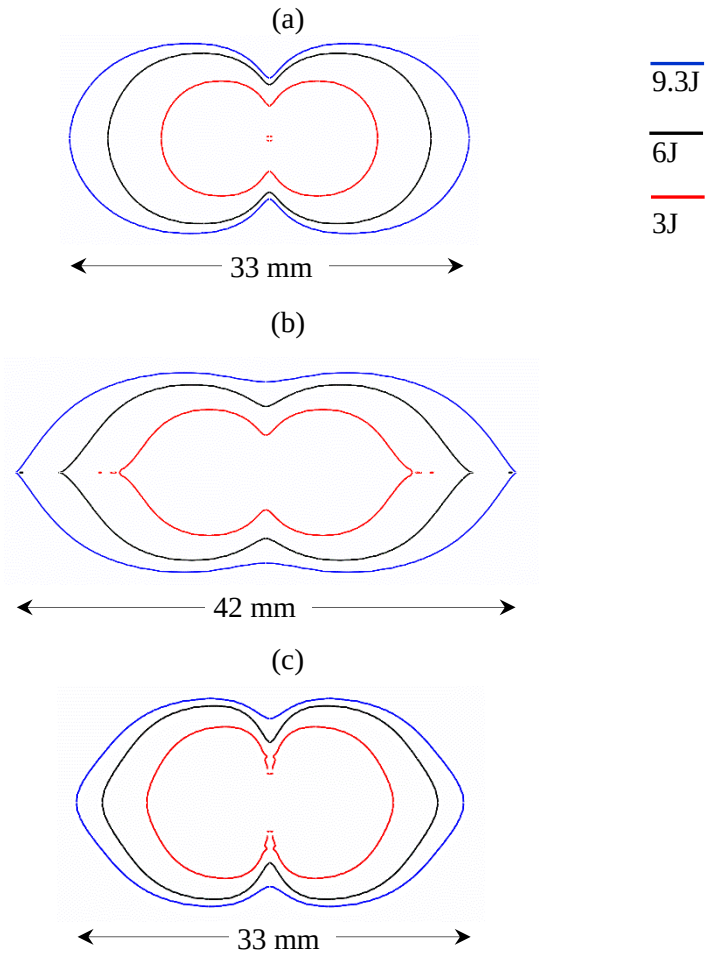

Figure 4 Delamination pattern at distal interface: (a) intra-laminar damage not accounted for; (b) intra-laminar damage represented by an embedded discrete crack; (c) CDM for the intra-laminar cracking.

Based on the analysis presented here, it can be concluded that the intra-laminar damage, i.e. the transverse matrix cracking in the 0° lamina distal to the impactor is the reason for the experimental observation of the pointed delamination tips. Without due consideration of this mode of damage, a rounded shape of delamination is predicted. Qualitatively, pointed tips of the delamination lobes can be captured by allowing intra-laminar damage development in the composite, either in form of dispersed damage, or a concentrated distinct crack. It is worth noting, however, that the latter approach has a limited predictive potential, since it implies that the location of the crack should be known in advance. As a result, its applicability to laminates of more complex lay-up cannot be assumed. Furthermore, the effects of such damage are exaggerated by a concentrated distinct crack, and a needle sharp delamination tip is predicted [9], which is not always realistic. On the other hand, it has been shown that the tendency of pointed tip subtlety can be captured simply by allowing the intra-laminar damage in the composite as a continuum. This method does not require the knowledge of the location of the transverse cracks in advance, hence can be applied to laminates of an arbitrary layup.

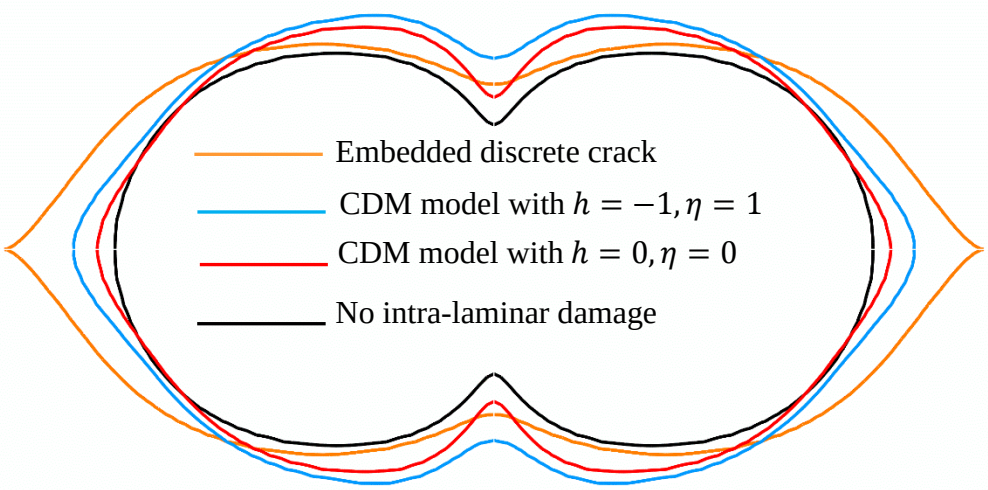

Figure 5. Comparison of delamination patterns in the lower interface at impact energy of 7J

5 CAPTURING THE INTACT ZONE BETWEEN THE LOBES OF DELAMINATION CAPTURING THE FEATURE OF POINTED DELAMINATION TIP

Accounting for intra-laminar damage growth in the composite allows predictions of the pointed tip of the delamination area, yet it does not assist in capturing the second delamination subtlety, which is the intact zone between the lobes of delamination.

5.1 Mesh refinement

On closer inspection of this area, an anomaly was identified in the prediction of the inter-laminar shear stress τ_{13}. Along the *y*-axis, it should assume zero values due to the symmetry condition as prescribed in the model. However, this was not quite the case in results, as can be seen in Figure 6(a), where a significant magnitude can be observed. It is well-known that stresses at the boundary are not generally predicted precisely from finite elements in the first place, and they are evaluated at the integration points off the boundary and extrapolated to the boundary. In presence of high stress gradient, which causes mesh sensitivity, such as the case of Figure 6(a), significant variations in stresses are present between the boundary and the integration points closest to the boundary. It resulted in the anomaly as observed in Figure 6(a). The issue was resolved by reducing the lengths of elements in *x*-direction near the centre of the plate. As can be seen in Figure 6(b), reasonable predictions of τ_{13} were produced with a model of the mesh refined locally. Mesh refinement also improved the predictions of damage in the centre of the interface layer. Comparing the damage contours produced by the models with the uniform and the refined mesh, as shown in Figure 7(a) at the same deformation level as that of Figure 6, it is easy to see that delamination contour became smoother. The further mesh refinement proposed here is in order to investigate the gap between the lobes of delamination. Otherwise, the mesh as shown in Figure 6 would be fine enough as pointed out before. In applications where this particular subtle feature of gap is not required, the proposed mesh refinement can be waived.

From the damage contour plot corresponding to the refined mesh in Figure 7(a), the intact zone between the two lobes of delamination seems to have been captured. However, this was only the case in the early stage of delamination, or when the laminate was subjected to a low energy impact. In fact, Figure 6 and Figure 7(a) represent an intermediate stage of deformation at a point when the projectile energy dissipated from its incident level of 6J to about 4.8J. On further loading, delamination area tends to expand in all directions, as can be seen in Figure 7(b). Towards the end of simulation, the surviving cohesive elements between the two lobes of delamination fail, the feature of intact zone disappears, and the damage contour corresponding to the model with a locally refined mesh becomes identical to that of the model with a uniform mesh. That was the reason why the necessity of further mesh refinement can

be easily overlooked in the conventional mesh convergence study. Therefore, in this case, mesh refinement alone delays the propagation of delamination towards the centre of the laminate, yet does not prevent it completely.

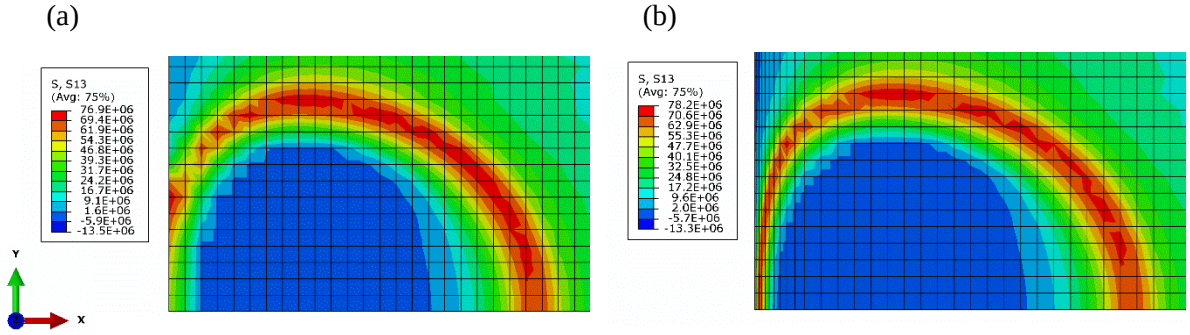

Figure 6 Contour of shear stress τ_{13} in cohesive layer at 90°/0° interface when impact energy is 6J: a) uniform mesh; b) refined mesh

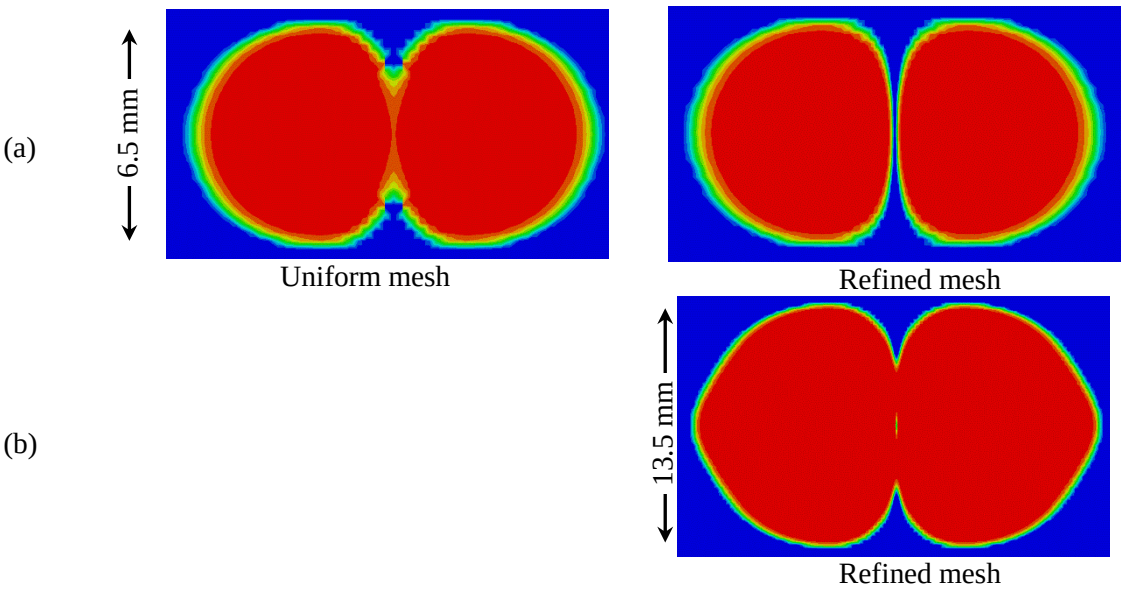

Figure 7 Predicted delamination under 6J impact energy: (a) comparison of the damage contours between uniform and refined meshes at the deformation level when the projectile energy has reduced to 4.8J from 6J (b) damage contour when projectile energy has reduced to 1.3J from 6J

As the direct stress transverse to the interface at centre is compressive and therefore does not contribute to delamination initiation and propagation, with transverse shear stress τ_{13} vanishing due to symmetry, the only remaining factor is the transverse shear stress τ_{23}. Examining the magnitude of this particular stress component, it can be found that it is not particularly high, but just high enough to trigger the delamination initiation and the subsequent propagation. A small amount of suppression will alter the outcome. This brings to our next consideration.

5.2 Friction

Within the cohesive interface, the shear stress τ_{23} is due to relative movement of 90° and distal 0° composite laminae, and it should vanish as well at the centre owing to the symmetry. Once the cohesive elements fail and the delamination occurs, composite layers on both sides of the failed cohesive elements come into direct contact, as the central zone of the laminate is subject to compression due to the pressing load. While the compression may not be high enough to suppress the delamination from taking place, it should result in a degree of friction resisting the shear, τ_{23}.

To introduce the frictional stress, the option available in Abaqus/Explicit [16] was employed to prescribe to tangential behaviour of contact surfaces, which is based on a penalty friction formulation. This requires definition of a single friction coefficient, μ. To investigate the influence of friction on delamination propagation, a number of laminate impact cases were simulated, where friction coefficient varied over a range as a parametric study, as presented in Figure 8.

As can be seen, the delamination area shrinks marginally as the friction coefficient increases. The most distinctive effect of friction on shape of the delamination pattern is the necking of delamination along *y*-axis, which becomes narrower as the friction coefficient increases. Eventually, at the friction coefficient between 0.2 and 1.0, the delamination splits into two disconnected lobes. Specifically, at maximum value of friction coefficient considered here, 5.0, gap can clearly be seen between the two lobes of delamination. This indicates that the frictional stress between delaminated surfaces helps to prevent delamination from propagating into the centre. This effect can only be captured with the synergy of refined mesh and consideration of friction between delaminated plies.

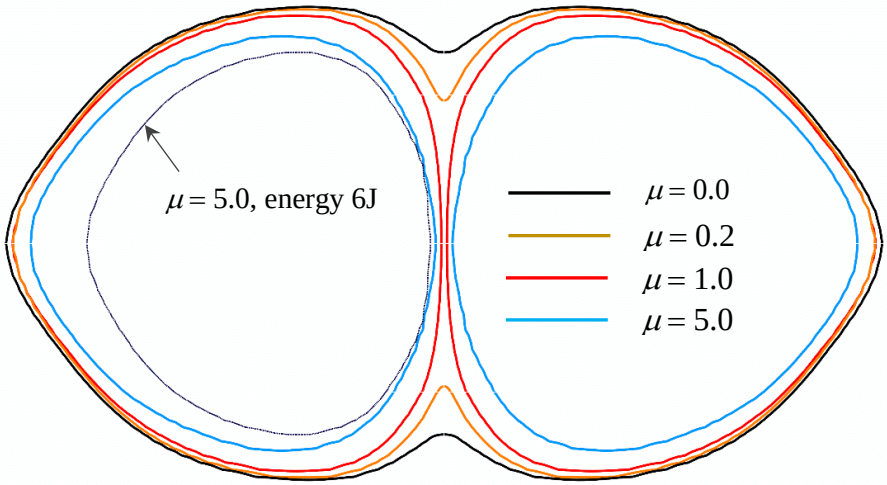

Figure 8. Delamination patterns at different values of friction coefficients when impact energy is 9.3J.

For comparison, delamination lobe outline, obtained numerically, corresponding to μ=5.0 at impact energy of 6J has also been added in Figure 8. As expected, the size of delamination in this case is smaller than at 9.3J, while the size of gap appears to have increased marginally.

It is worth noting that the values of friction coefficients employed here were meant to facilitate the parametric study, in absence of physically measured ones, although attempts of having them experimentally measured have been reported in the literature [20]. As there is a wide range of factors affecting the roughness of the delamination surface, such as the composite system, the interlaminar interface design and quality, the nature of the impact, the anisotropy of the friction characteristics, etc., it is not practical yet to base the analysis on measured friction coefficients. The range selected was not meant to stand physical scrutiny. Rather, it might pre-empt physical possibilities without conducting sophisticated experiments.

5.3 The width of the intact gap

Even though the gap feature can be captured by accounting for the friction in the simulation, the predicted width of the gap is relatively small as compared to that observed in the experiments [6]. The reason is believed to be the lack of localised Hertzian indentation, which cannot be reflected in models using any kind of shell elements. Such local deformation in reality allows the load to be distributed over a significantly larger area under the impactor, and the width of the intact zone in reality is expected to be larger than that predicted. Without reverting to the formidable simulation using solid elements at a very fine mesh, an alternative is attempted by artificially increasing the diameter of the impactor, understanding that it is not a very effective way of increasing the size of the contact area.

A simulation was conducted, where the diameter of the impactor was increased to 30mm. Delamination patterns obtained with the two sizes of the impactor are compared in Figure 10. With the use of 30 mm impactor, the gap size increased by a factor of three, even though the absolute magnitude is still very small. The message is clear that the local distribution of the impact force over the part of the laminate underneath the impactor plays a significant role in determination of the size of the gap. With increased impactor radius, the length and the width of the delamination have also increased but only marginally.

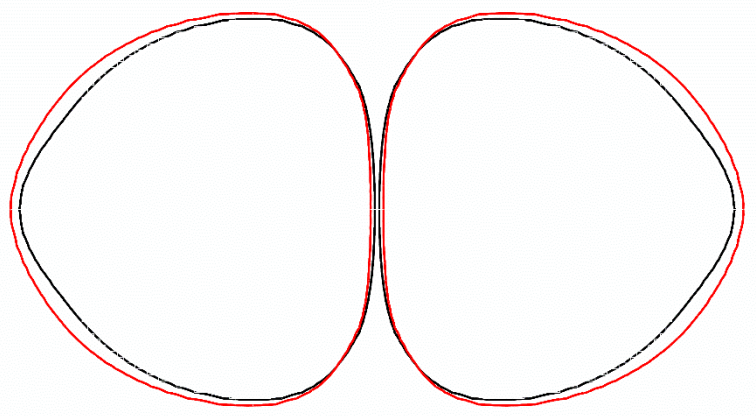

Figure 9. Intact zone between the delamination lobes at two different diameters of the impactor (friction coefficient 1.0, impact energy 9.3J).

This study indicates that the quantitative predictions of the size of the intact zone would require more accurate way of simulating the Hertzian contact between the impactor and the laminate. However, the qualitative feature of an intact zone under the impactor can be captured confidently by the synergy of incorporating the friction between the delaminated interlaminar surfaces and a reasonably refined mesh.

6 CONCLUSIONS

The reasons behind the two subtle features of delamination patterns in cross-ply laminates subjected to impact, viz. the pointed delamination fronts and an intact zone underneath the impactor, as are commonly observed experimentally, have been identified for the first time. They have been illustrated through examples with logical reasoning, such that these features can be consistently captured when the appropriate considerations for them are accounted for in the numerical model.

It has then be demonstrated clearly that the pointed delamination tips in numerical modelling are attributed to the incorporation of the intra-laminar damage, i.e. transverse matrix cracking, micro or macro, in the distal 0° lamina from the impactor. This feature can therefore be consistently captured, provided that the damage-related material properties are so given that they allow the transverse matrix cracking to take place and to evolve. Otherwise, rounded ends of delamination will be predicted.

The synergy of sufficiently refined meshes and the effects of friction between the delaminated interfaces enables the numerical model to capture the intact zone under the impactor as another subtle feature consistently observed in experiments.

The features addressed in this paper may be classified as of secondary significance as compared to the delamination area and the dimensions. However, the successful identification of the reasons behind them and the ability to reproduce them theoretically help profoundly in building up the level of confidence of theoretical prediction of delamination in a much broader sense. Based on such an enhanced level of confidence, users now can have the choice of incorporating higher levels of sophistication in order to capture features of such subtlety, when they become necessary. Alternatively, if the application concerned does not need information of this level of subtlety, one can confidently reduce the level of sophistication and hence the computational demands, yet to obtain satisfactory results suitable for the application.

ACKNOWLEDGEMENTS

The financial support for the work carried out from Beijing Institute of Aeronautical Materials (BIAM), China under Contract Number RGS 107903 is gratefully acknowledged.

REFERENCES

[1] S. Abrate, Impact on composite structures, Cambridge University Press, UK, 1998.
[2] ASTM International Standard Test Method for Measuring the Damage Resistance of Fiber-Reinforced Polymer Matrix Composite to a Drop-Weight Impact Event. 2015
[3] S. Long, X. Yao, X. Zhang, Delamination prediction in composite laminates under low-velocity impact, *Composite Structures*, **132** (2015) 290–298
[4] H.Y. Choi, Chang FK, A model for predicting damage in graphite/epoxy laminated composites resulting from low-velocity point impact, *J. Compos. Mater*. **26**(14) (1992) 2134–69
[5] Y. Shi, T. Swait, C. Soutis Modelling damage evolution in composite laminates subjected to low velocity impact, *Composite Structures* **94** (2012) 2902–2913
[6] Aymerich, F., C. Pani, and P. Priolo, *Damage response of stitched cross-ply laminates under impact loadings. Engineering Fracture Mechanics*, **74**(4) (2007) 500-514
[7] R.K. Luo, E.R. Green, C.J. Morrison, Impact damage analysis of composite plates, International *Journal of Impact Engineering*, 22 (1999) 435-447
[8] S. Li, S.R. Reid, Z. Zou, Modelling damage of multiple delaminations and transverse matrix cracking in laminated composites due to low velocity lateral impact. *Composites Science and Technology*, **66** (2006) 827-836
[9] Aymerich, F., F. Dore, and P. Priolo, Prediction of impact-induced delamination in cross-ply composite laminates using cohesive interface elements. *Composites Science and Technology*, **68**(12) (2008) 2383-2390
[10] Aymerich, F., F. Dore, and P. Priolo, Simulation of multiple delaminations in impacted cross-ply laminates using a finite element model based on cohesive interface elements. *Composites Science and Technology*, **69**(11–12) (2009) 1699-1709
[11] A. Qiu, K. Fu, W. Lin a, C. Zhao, Y. Tang, Modelling low-speed drop-weight impact on composite laminates, *Materials and Design* **60** (2014) 520 – 531
[12] Zhang, J. and Zhang, X., Simulating low-velocity impact induced delamination is composites by a quasi-static load model with surface-based cohesive contact. *Composite Structures*, **125** (2015) 51--57
[13] X. Zhang, F. Bianchi and H.Liu, Predicting low-velocity impact damage in composites by a quasi-static load model with cohesive interface elements. *The Aeronautical Journal*, **116**(1186) (2012) 1367-1281
[14] G Perillo, NP Vedivik and AT Echtermeyer, Damage development in stitch bonded GFRP composite plates under low velocity impact: Experimental and numerical results, *J. Compos. Mater.* **49**(5) (2015) 601–615
[15] United States Government Accountability Office, Status of FAA's Actions to Oversee the Safety of Composite Airplanes, 2011, Report to Congressional Requesters.
[16] Abaqus Analysis User's Manual. Abaqus 6.12 HTML Documentation, 2012.
[17] S. Li, S.R. Reid and P.D. Soden, A continuum damage model for transverse matrix cracking in laminated fibre-reinforced composites. *Philosophical Transaction of the Royal Society A: Mathematical, Physical and Engineering Science*, **356**(1746) (1998) 2379-2412
[18] Li, S., Reid, R.S., Soden P.D. and Hinton MJ, Modelling transverse cracking damage in thin, filament-wound tubes subjected to lateral indentation followed by internal pressure. *International Journal of Mechanical Sciences*. **47** (2005) 621-646
[19] R. Talreja, A continuum mechanics characterization of damage in composite materials. *Proceedings of the Royal Society of London A*, **339** (1985) 195–216
[20] J. Schön, Coefficient of friction of composite delamination surfaces, *Wear*. **237** (2000) 77–89